Non-linear hybrid homogenization method for steel-reinforced resin

Nijgh, Martin; Xin, Haohui; Veljkovic, Milan

DOI
10.1016/j.conbuildmat.2018.06.111

Publication date
2018

Document Version
Final published version

Published in
Construction and Building Materials

Citation (APA)
Nijgh, M., Xin, H., & Veljkovic, M. (2018). Non-linear hybrid homogenization method for steel-reinforced resin. *Construction and Building Materials*, *182*, 324-333. https://doi.org/10.1016/j.conbuildmat.2018.06.111

Construction and Building Materials 182 (2018) 324–333

Contents lists available at ScienceDirect

Construction and Building Materials

journal homepage: www.elsevier.com/locate/conbuildmat

Non-linear hybrid homogenization method for steel-reinforced resin

Martin Paul Nijgh, Haohui Xin *, Milan Veljkovic

Faculty of Geoscience and Engineering, Delft University of Technology, Netherlands

HIGHLIGHTS

- A prediction method for mechanical behaviour of steel-reinforced resin is derived.
- Steel-reinforced resins are superior to conventional resins in terms of stiffness.
- Body-centred cubic sphere packing is representative for random sphere disposition.
- Positive influences due to confinement effects depend mainly on Poisson ratio.

ARTICLE INFO

Article history:
Received 23 April 2018
Received in revised form 12 June 2018
Accepted 13 June 2018
Available online 20 June 2018

Keywords:
Injected bolted connections
Steel-reinforced resin
Hybrid homogenization method
Confinement effects

ABSTRACT

Injected bolted connections have been used in the Netherlands since the 1970s, initially to replace riveted connections of steel railway bridges. More recently, structural components with different geometrical tolerances have also been connected using injection bolts and oversize holes. The natural confinement of a bolted connection provides support to the injected epoxy resin so that it can withstand bearing stresses that are significantly higher than its uniaxial compressive strength. A recent innovation in the field of injected bolted connections is the development of steel-reinforced resin, which consists of a skeleton of steel particles and a conventional epoxy resin (polymer). In previous research, the steel-reinforced resin has shown to increase the connection stiffness and decrease creep deformation significantly. In this paper, a hybrid analytical-numerical homogenization method, which can consider the plasticity of steel and resin, is proposed to determine the stress-strain relationship of steel-reinforced resins. The results of the hybrid homogenization method are validated against experimental data of small-scale specimen, subjected to compression in unconfined and confined conditions. Proposed hybrid homogenization method is an alternative to complex multi-scaling methods and allows for quick but accurate determination of mechanical properties of steel-reinforced resins.

1. Introduction

Injected bolted connections (IBCs) are conventional bolted connections of which the remaining bolt-to-hole clearance is injected with an epoxy resin through a standardized, modified bolt, as illustrated through Fig. 1. IBCs have been used in the Netherlands since the 1970s, initially to replace riveted connections of steel railway bridges. Two main reasons for the use of IBCs were:

- riveting was no longer common practice;
- determination of the actual slip factor of the faying surfaces in case of refitting with preloaded bolts is not possible.

Recently, a paper published by de Oliveira Correia et al. [1] addressed the application of IBCs in renovation of bridges, provided statistical analysis of fatigue experiments and identified needs for furthers studies related to fatigue classification.

Injected bolted connections can be used for two main types of applications: either to obtain a slip-resistant steel-to-steel connection (e.g. as an alternative to preloaded connections) [2] or to obtain a stiff connection between components with different geometrical deviations (e.g. steel and concrete) [3]. In the latter application, oversize holes are used to allow for greater positioning tolerances.

The epoxy resin system that is generally used in injected bolted connections (IBCs) is the commercially available RenGel SW 404 + HY 2404. Recent research of Koper [4] on steel-to-steel IBCs has indicated that this epoxy resin system performs best in comparison to a selection of alternative resins. Wedekamper [5] investigated the mechanical properties of this resin in detail through a series

* Corresponding author.
E-mail address: H.Xin@tudelft.nl (H. Xin).

https://doi.org/10.1016/j.conbuildmat.2018.06.111
0950-0618/

Nomenclature

d	diameter
D	damage variable
E_1	Young's Modulus of particles
E_2	Young's Modulus of matrix
$E_{c,lower}$	lower bound for Young's Modulus of composite material
$E_{c,upper}$	upper bound for Young's Modulus of composite material
E_r	Young's Modulus of resin matrix
E_s	Young's Modulus of steel particle
E_{s+r}	Young's Modulus of steel-reinforced resin
$h_r(x_i, y_j)$	total height of resin matrix in element (x_i, y_j)
$h_s(x_i, y_j)$	total height of steel particles in element (x_i, y_j)
$h_{s,p}(x_i, y_j)$	height of the p-th steel particle in element (x_i, y_j)
$k_{eq}(x_i, y_j)$	equivalent spring stiffness of element (x_i, y_j)
$k_r(x_i, y_j)$	spring stiffness of matrix component of element (x_i, y_j)
$k_s(x_i, y_j)$	spring stiffness of steel component of element (x_i, y_j)
l	length
m	mass
n	number of discrete elements within unit cell along x and y axes
q	number of spheres in unit cell
r	sphere radius
u_0	imposed longitudinal contraction of unit cell
$u_r(x_i, y_j)$	longitudinal contraction of resin spring in element (x_i, y_j)
$u_s(x_i, y_j)$	longitudinal contraction of steel spring in element (x_i, y_j)
V	volume
V_f	volume fraction of particles
X	parameter

Greek letters

Δu_{max}	maximum difference between imposed and actual contraction of unit cell
$\varepsilon_r(x_i, y_j)$	resin strain in element (x_i, y_j)
$\varepsilon_s(x_i, y_j)$	steel strain in element (x_i, y_j)
ε_{thr}	threshold strain after which damage develops
ν_{s+r}	Poisson ratio of steel-reinforced resin
ρ_r	density of resin matrix
ρ_s	density of steel particle
σ_D	stress in damaged element
σ_{s+r}	stress in steel-reinforced resin

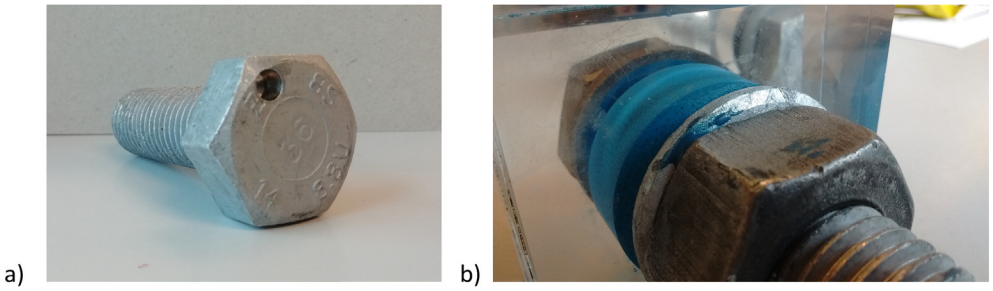

Fig. 1. (a) M20 × 50 mm ISO4017 8.8U bolt with an injection channel in the bolt head. (b) Resin-injected bolted connection with transparent plate package. The resin (blue) is injected through a hole in the bolt head. (For interpretation of the references to colour in this figure legend, the reader is referred to the web version of this article.)

of compression, tension, shear and pull-out tests. Nijgh [6] has suggested reinforcing commercially available resins using steel particles in order to increase connection stiffness and to decrease creep deformation. In this perspective, steel shot has a good potential as the reinforcing material, given that this product is widely available on the market because of its application in steel blasting.

The material behaviour of reinforced resin depends on the type of resin, type of the reinforcing material and the volume fraction thereof. It is important to adopt a multi-scale analysis to determine the mechanical properties of the steel-reinforced resin. Generally, multi-scale homogenization methods are subdivided into analytical and numerical methods. After decades of effort, several analytical methods of continuum micromechanics have been developed, including Voigt's model [7], Reuss' model [8], Vanishing Fiber Diameter (VFD) model [9], Composite Cylinder Assemblage (CCA) model [10,11], Hashin-Shtrikman Bounds [12,13], Self-Consistent Schemes [14,15] and the Mori-Tanaka Method [16,17]. The unit cell complexity and non-linear behaviour of the constituent materials make the analytical micromechanics methods cumbersome for non-linear predictions. Compared with analytical micromechanics formulations, numerical homogenization simulations can accurately consider the geometry and spatial distribution of the phases, and can also accurately estimate the propagation of damage to predict the failure strength [18]. Macroscopic material properties of the composites can be determined by means of numerical modelling of deformation and failure of the assumed microstructural model, which is considered through a representative volume element (RVE). A downside of numerical homogenization methods is that they are computationally expensive, as frequently reported in the literature [19,20,21]. A combination of analytical micromechanics methods and numerical homogenization methods is expected to consider the complexity of constituent materials and spatial distribution of phases in a unit cell, at little computational cost.

The goal of this paper is to demonstrate a hybrid analytical-numerical homogenization method, which is less mathematically strict compared to traditional homogenization methods, but can be effectively used to determine the compressive stress-strain relationship of steel-reinforced resins. The hybrid homogenization model is validated against experimental data obtained from a small-scale specimen, subjected to compression in confined and unconfined conditions. In addition, an analytical method is derived to determine the degree of confinement and it is investigated which parameters have the largest influence on the apparent longitudinal Young's Modulus. Finally, conclusions are drawn on the effectiveness of the reinforcing particles through a parameter study on the effects of the steel volume fraction on the Young's Modulus of the composite material.

2. Methodology

2.1. Hybrid homogenization method

Theoretical upper and lower bounds of Young's Modulus of two-phase composite materials are respectively defined by Eqs. (1) and (2). The upper bound for the Young's Modulus is based on the assumption that the constituent materials are oriented in the direction of loading (Voigt model [7]), whereas for the lower bound it is assumed that these are oriented perpendicular to the direction of loading (Reuss Model [8]).

$$E_{c,lower} = \left(\frac{V_f}{E_1} + \frac{1 - V_f}{E_2}\right)^{-1} \tag{1}$$

$$E_{c,upper} = V_f \cdot E_1 + (1 - V_f) \cdot E_2 \tag{2}$$

In Eqs. (1) and (2), V_f and $1 - V_f$ denote the volume fractions of materials with Young's Modulus E_1 and E_2, respectively. Given that in steel-reinforced resin neither the assumptions from the Voigt or Reuss models are fulfilled, it follows that actual Young's Modulus must be in between the upper and lower bounds. To determine the actual stress-strain relationship of steel-reinforced resin, a hybrid (analytical-numerical) homogenization method is developed.

A three-dimensional unit cell with a certain dispersion of reinforcing shot particles is assumed to represent the actual packing of the spheres in a connection or specimen. The dispersion of spheres is assumed to be in the form of a body-centred cubic packing (see Fig. 2), as frequently adopted in literature. Given the volume fraction V_f of reinforcing spherical particles and the number of spheres q in the unit cell, the sphere radius r can be determined by Eq. (3).

$$r = \sqrt[3]{\frac{1}{q} \cdot \frac{3}{4} \frac{V_f}{\pi}} \tag{3}$$

$$V_f = \frac{\frac{m}{V} - \rho_r}{\rho_s - \rho_r} \tag{4}$$

The volume fraction of the reinforcing particles can be determined by Eq. (4), in which m and V represent the mass and volume of the specimen, respectively, and ρ_r and ρ_s denote the density of the matrix (resin) and particles (steel spheres), respectively. For a Body-centred cubic packing, $q = 2$ and the maximum volume fraction of spheres is approximately 68%.

To validate the assumption that a body-centred cubic packing of spheres is representative for the actual dispersion of spheres in steel-reinforced resin, a larger cell with more spherical particles is considered. Several methods are available in literature that are capable of randomly distributing spherical particles, e.g. the Dropping and Rolling Method [22], the Optimized Dropping and Rolling Method [23] and the Gravitational Sphere Packing Method [24]. All aforementioned models require the definition of several algorithms, e.g. to determine if spheres are touching, whether the position of the sphere is stable, how a stable sphere positon can be achieved, etc. To simplify the generation of a random-packed sphere skeleton, the gravity principle of the Gravitational Sphere Packing Method is utilized, but the dropping of, and interaction between, spheres is proposed to be solved using 3D simulation software. The simulation package Blender [25] is used to automatically solve all contact and other interaction phenomena. A large number of identical spheres is generated and dropped into a rectangular container, the result of which is shown in Fig. 3. The remaining voids are assumed to be filled with resin. The mechanical behaviour of the generated 3D sphere skeleton is analysed using the same method as for the unit body-centred cubic cell. This method is outlined in the following. The Young's Modulus of steel-reinforced resin based on the generated sphere skeleton is determined over the entire skeleton height (~15 mm) for various cross-sectional dimensions within the 6 mm by 6 mm skeleton cross-section. This variation in cross-sectional dimensions is carried out is to obtain insight in the influence of boundary conditions on the Young's Modulus.

The unit cell is subdivided into n by n ($=n^2$) equally sized elements in the x-y plane, see Fig. 3. Based on the assumed volume fraction and dispersion of the reinforcing spheres, the total height of the reinforcing spheres for each of the n^2 elements on the x-y plane can be determined by Eq. (5). The remainder of the unit cell is then assumed to be filled with resin, therefore the height of the resin can be determined by Eq. (6).

$$h_s(x_i, y_j) = \sum_{p=1}^{q} h_{s,p}(x_i, y_j) \tag{5}$$

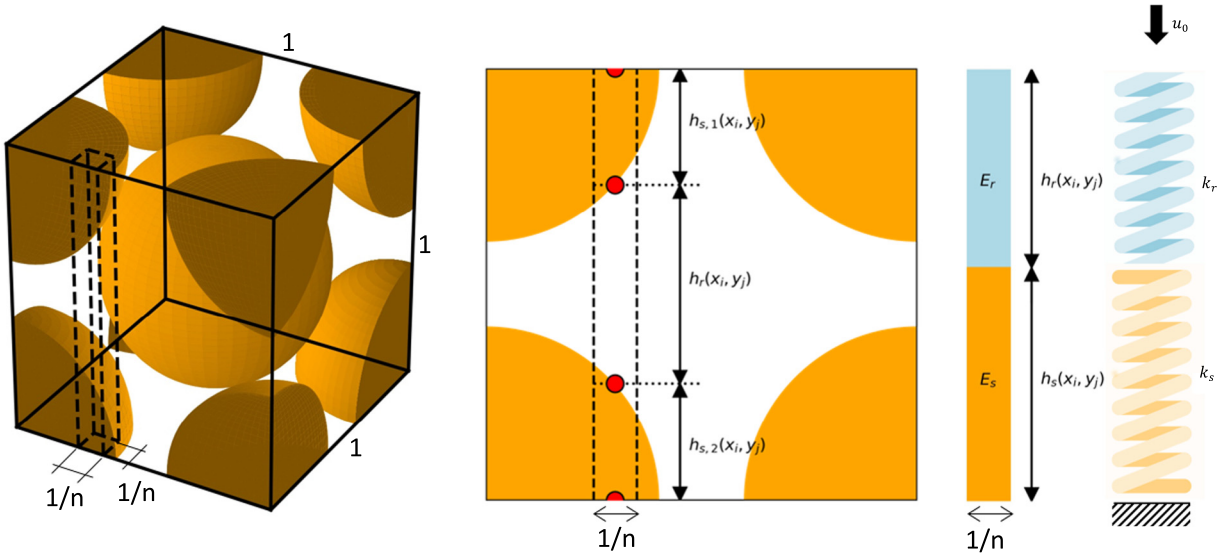

Fig. 2. Left: Body-centered cubic arrangement of reinforcing steel spheres, indicating a discrete element with size 1 × 1/N × 1/N within the unit cell. Middle: cross-sectional view at the center of the discrete element. Right: conversion of the discrete element into a set of two serial springs.

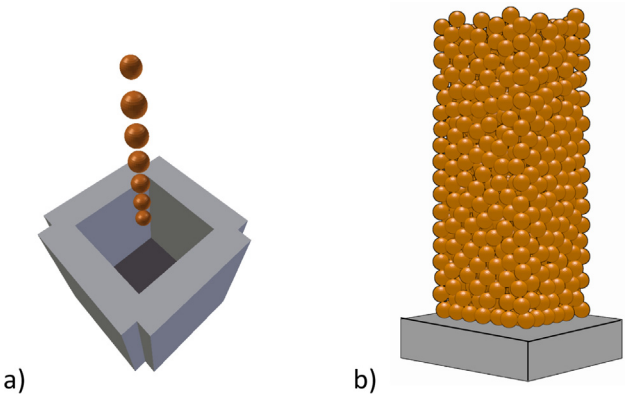

Fig. 3. (a) Simulation using Blender [25], in which spheres of equal size are dropped from a stock into a rectangular box, the software automatically detects and solves contact and other interaction phenomena. (b) Generated skeleton of spheres.

$$h_r(x_i, y_j) = 1 - h_s(x_i, y_j) \tag{6}$$

The resin and steel are modelled as two springs in series for each of the n^2 elements, see Fig. 2. The spring stiffness of the steel and resin parts in each element can be determined by Eqs. (7) and (8), respectively.

$$k_s(x_i, y_j) = \frac{E_s \cdot \frac{1}{n^2}}{h_s(x_i, y_j)} \tag{7}$$

$$k_r(x_i, y_j) = \frac{E_r \cdot \frac{1}{n^2}}{h_r(x_i, y_j)} \tag{8}$$

In Eqs. (7) and (8), E_s and E_r respectively denote the Young's Modulus of the steel and resin. The equivalent spring stiffness of these two springs in series is given by Eq. (9). The Young's Modulus of the steel-reinforced resin can be computed by summing the equivalent spring stiffness of all n^2 elements, as expressed through Eq. (10).

$$k_{eq}(x_i, y_j) = \frac{k_r(x_i, y_j) \cdot k_s(x_i, y_j)}{k_r(x_i, y_j) + k_s(x_i, y_j)} \tag{9}$$

$$E_{s+r} = \sum_{j=1}^{n} \sum_{i=1}^{n} k_{eq}(x_i, y_j) \tag{10}$$

The non-linear behaviour of each of the constituent materials can be implemented to determine the non-linear branch of the stress-strain relationship of the two-phase material. An axial deformation u_0 is applied to each element within the unit cell. A trial solution of the deformation of the resin in each of the n^2 elements is assumed, e.g. through the analytical solution for the linear-elastic stage, as defined in Eq. (11). The strain in the resin layer can then be computed through Eq. (12), based on which the corresponding stress $\sigma(x_i, y_j)$ can be derived through its stress-strain curve.

$$u_r(x_i, y_j) = \frac{u_0}{1 + \frac{k_r(x_i, y_j)}{k_s(x_i, y_j)}} \tag{11}$$

$$\varepsilon_r(x_i, y_j) = \frac{u_r}{h_r(x_i, y_j)} \tag{12}$$

Based on the determined stress $\sigma(x_i, y_j)$, the deformation of the steel $u_s(x_i, y_j)$ can be computed via its stress-strain curve and Eq. (13).

$$u_s(x_i, y_j) = \varepsilon_s(x_i, y_j) \cdot h_s(x_i, y_j) \tag{13}$$

The total actual deformation then amounts to $u_r(x_i, y_j) + u_s(x_i, y_j)$. Iteration is carried out until the difference between the applied deformation and actual deformation is sufficiently small:

$$\left| u_0 - \left[u_r(x_i, y_j) + u_s(x_i, y_j) \right] \right| < |\Delta u_{max}| \tag{14}$$

When Eq. (14) is valid, the stress $\sigma(x_i, y_j)$, for that particular element is recorded. After iterating for all of the n^2 elements, the stress and strain of the two-phase material can be determined by Eqs. (15) and (16), respectively.

$$\sigma_{s+r} = \frac{1}{n^2} \cdot \sum_{j=1}^{n} \sum_{i=1}^{n} \sigma(x_i, y_j) \tag{15}$$

$$\varepsilon_{s+r} = u_0 \tag{16}$$

Carrying out above procedure for a sufficient number of deformations u_0, the stress-strain curve of the steel-reinforced resin

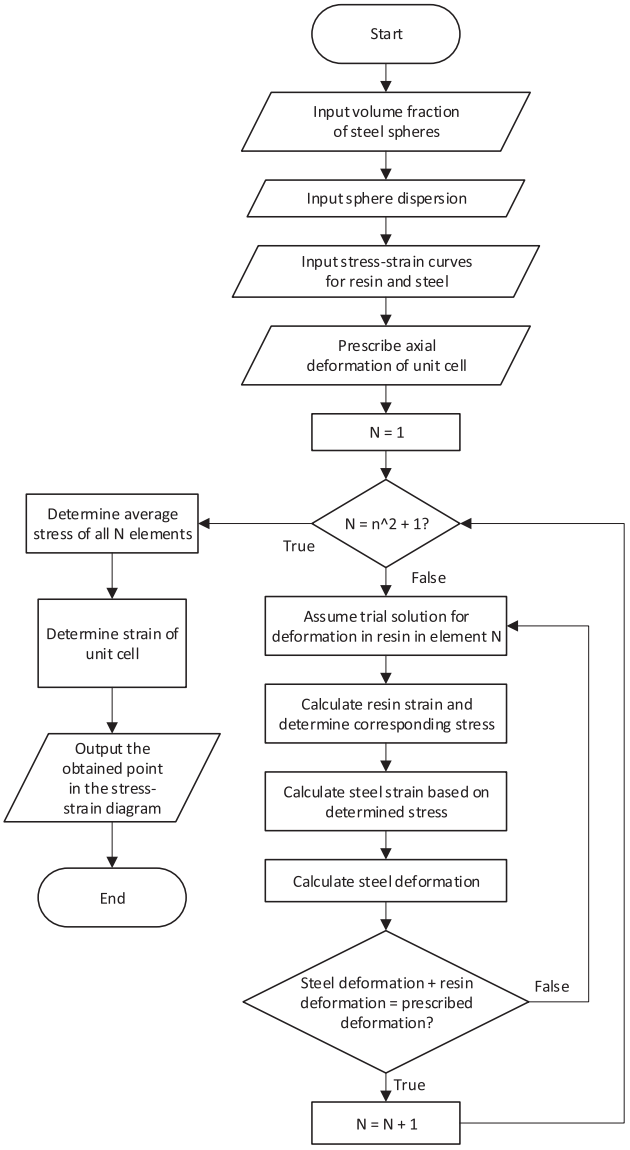

Fig. 4. Flowchart of the hybrid homogenization model for the determination of a point on the stress-strain curve of steel-reinforced resin. Repetition of the process for multiple prescribed axial deformations provides the complete stress-strain curve.

can be derived. The process of the determining a point in the stress-strain curve of steel-reinforced resin is clarified through the flowchart illustrated in Fig. 4.

2.2. Unconfined specimen

To validate the aforementioned approach, a series of compression tests on cylindrical specimen is conducted in unconfined condition. A load is applied using a stroke-controlled regime at a speed of 0.01 mm/s. Two Ono Sokki GS-551 linear gauge sensors with a range of 0.001–5 mm were used to measure the axial deformation of the specimen.

An overview of the experimental test specimens is given through Table 1. The experimental set-up is illustrated through Fig. 5.

RenGel SW 404 with hardener HY 2404 was used as the epoxy resin since its use in IBCs is well-established in the construction industry. Earlier work of Koper [4], Nijgh [6] and Wedekamper [5] indicate that the spread in mechanical properties is sufficiently small to justify a limited number of material tests.

Reinforcing particles were chosen as steel shot S330 ($Ø_{nom}$ = 0.84 mm) complying with standards SAE J872 [26] and J444 [27]. The target was to achieve a loose random packing by pouring the spheres into a mould, which generally corresponds to a fraction of steel shot of approximately 60%.

The aspect ratio l/d is chosen such that the effect of interface friction on the Young's Modulus is sufficiently small (<2%) according to the theory of Williams & Gamonpillas [28]. Given that the specimens are unconfined, the prediction for the stress-strain curve of steel-reinforced resin is exactly conform Eqs. (15) and (16).

One resin and one steel-reinforced specimen have been instrumented with strain gauges in axial and tangential directions to determine the Poisson ratios. The prediction of the Poisson ratio is complex for two-phase composite materials since the Poisson ratio of the composite is not only bounded by the Poisson ratio of the constituent materials. Several methods and theories have been derived, e.g. by Zimmerman [29] focusing on stiff spherical inclusions in a relatively compliant matrix. Hsieh & Tuan [30] have derived a model for two-phase composites, in which the Poisson ratio of the composite material is derived by Eqs. (17) and (18). In these equations, v denotes the Poisson ratio and subscripts s and r relate to particle (steel) and matrix (resin) properties, respectively. The model of Hsieh & Tuan [30] is implemented in each of the n^2 elements to obtain the homogenized (averaged) Poisson ratio of the unit cell.

$$v_{s+r} = \frac{[(1-v_s)E_r - (1-v_r)E_s](1-V_f) + (v_r(1-V_f)E_s + v_s V_f E_r)X}{2(v_s E_r - v_r E_s)(1-V_f) + ((1-V_f)E_s + V_f E_r)X} \tag{17}$$

$$X = \frac{(1-v_r)E_s V_f + (1-v_s)E_r(1-V_f)}{(v_r E_s - v_s E_r)V_f} \tag{18}$$

2.3. Confined specimen

In addition to the unconfined specimen series, also tests are carried out on confined specimen. The composition of these specimen and the testing protocol is identical to that of the unconfined specimen, only the specimen dimensions differ (see Table 1).

The specimens are passively confined through the use of a Ø30 mm × 50 mm S235 steel tube with a wall thickness of 4 mm. The load is transferred from the jack to the specimen through a Ø22 × 40 mm solid cylinder with a snug fit in the steel tube.

Previously, Nijgh [6] has shown that the apparent longitudinal Young's Modulus $E_{c,100\%,x}$ increases significantly with the Poisson ratio v under on the assumption of perfect confinement conditions, as expressed through Eq. (19).

$$\frac{E_{c,100\%,x}}{E} = \frac{1-v}{1-v-2v^2} \tag{19}$$

An analytical relationship is derived to take into account that lateral expansion is not fully restrained in the current specimen design. Based on Hooke's law and the definition of hoop strain (Eq. (20)) for thin-walled cylinders, the apparent longitudinal Young's Modulus $E_{c,x}$ of partially confined materials can be expressed through Eq. (21), using that $\varepsilon_{yy} = \varepsilon_{zz} = \varepsilon_{hoop}$. In Eq. (21), d_{cyl}, t_{cyl} and E_{cyl} denote the average diameter ($d_{cyl} = d - t$), wall thickness and Young's Modulus of the confining cylinder, respectively.

$$\varepsilon_{hoop} = -\frac{1}{E_{cyl}}\frac{v\sigma_{xx}d_{cyl}}{2t_{cyl}} \tag{20}$$

$$\frac{E_{c,x}}{E} = \max\left[\frac{1}{-\frac{v^2(Ed_{cyl}-2E_{cyl})}{t_{cyl}E_{cyl}\cdot(v-1)}+1}, 1\right] \tag{21}$$

Eq. (21) goes to the analytical upper bound solution of the apparent longitudinal Young's Modulus $E_{c,100\%,x}$ for $d \to 0$ and/or $t \to \infty$ and to the Young's Modulus of the unconfined material for $t \to 0$ and/or d $\to \infty$. Fig. 6 illustrates the effect of the thickness and diameter on the apparent Young's Modulus $E_{c,x}$ for E = 5.64 GPa, v = 0.315 and d = 26 mm. The apparent Young's modulus increases progressively with an increase in the Poisson ratio, whereas the confinement conditions itself have a less dominating effect in case of materials with a relatively low Young's Modulus, as illustrated through Fig. 7. The properties of the confining cylinder can compensate for each other, i.e. a confining cylinder with a t_{cyl} = 4 mm and E_{cyl} = 210 GPa provides confinement equally well as a cylinder with t_{cyl} = 8 mm and E_{cyl} = 105 GPa.

The non-linear behaviour of the confined specimen is not considered analytically, since this occurs at stress ranges in which

Table 1
Test matrix of small-scale specimen.

	Nominal geometry	Number of tests	
		Resin	Steel-reinforced resin
Unconfined	Ø26.3 mm × 50 mm	5	5
Confined	Ø22 mm × 22 mm	5	5

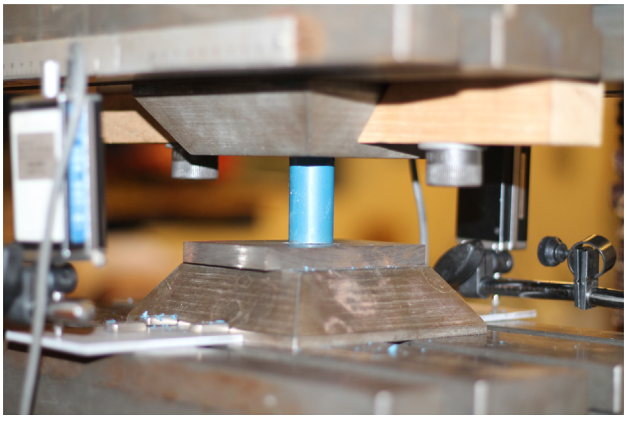

Fig. 5. Unconfined resin specimen in the experimental set-up of the compression test.

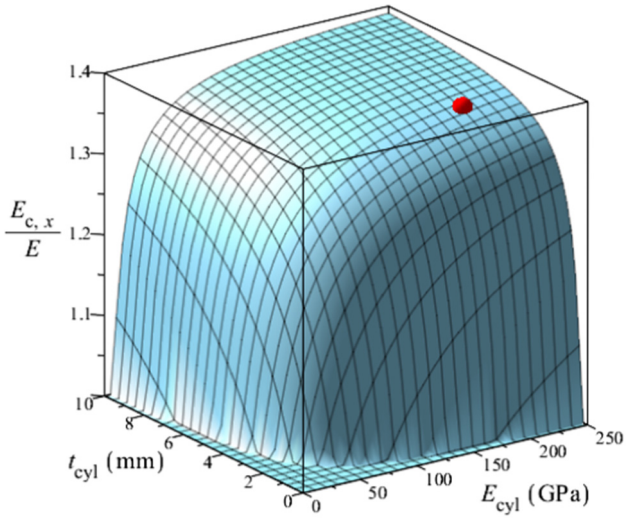

Fig. 6. Effect of confinement on the apparent Young's Modulus for $E = 5.64$ GPa, $\nu = 0.315$ and $d_{cyl} = 26$ mm and a confining cylinder with certain wall thickness t_{cyl} and Young's Modulus E_{cyl}. Marker indicates the conditions under which the confined resin specimen were tested.

the confining cylinder starts yielding. Therefore, only prediction of the Young's Modulus is made based on Eq. (21).

3. Experimental results and analysis

3.1. Unconfined specimen

The engineering stress-strain curves for unconfined resin and steel-reinforced resin are illustrated through Figs. 8 and 9, respectively. The Young's Modulus and strength of these specimen are summarized in Table 2 and Table 3, respectively. Representative determination of Young's Moduli was done over an interval of 40 MPa (approximately one-third of the stress at the onset of non-linearity for unconfined specimen) for which the slope of the curve is largest, to avoid influence due to accuracy of recorded data.

The Poisson ratios of the resin and steel-reinforced resin are determined as 0.315 and 0.22, respectively.

The approximated bi-linear stress-strain curve of the unconfined resin is used as input for the hybrid homogenization model that was developed to predict the stress-strain relationship for unconfined steel-reinforced resin. The experimental as

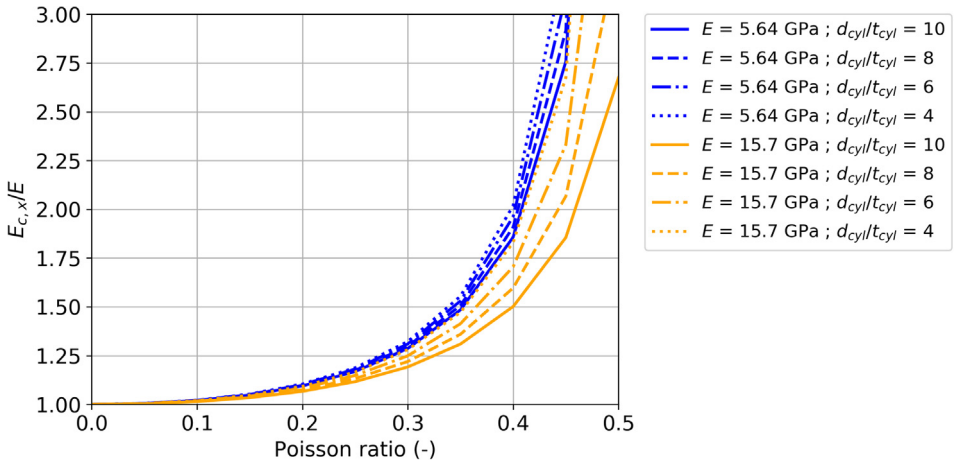

Fig. 7. Apparent Young's Modulus as a function of material Young's Modulus and ratio of cylinder diameter over wall thickness. It is assumed that Young's Modulus of the cylinder is 210 GPa.

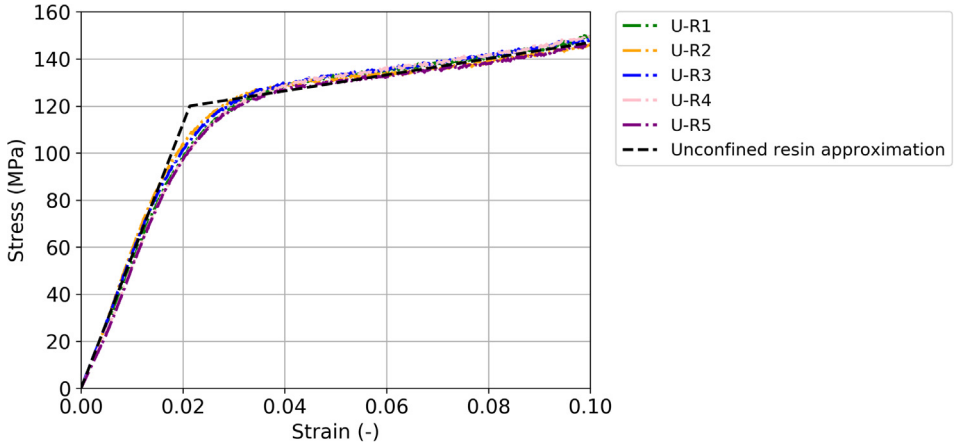

Fig. 8. Stress-strain curve for unconfined resin specimen.

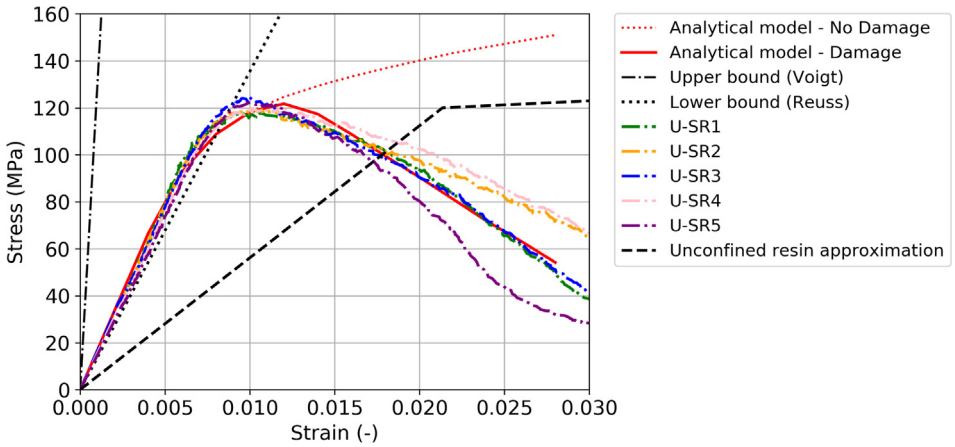

Fig. 9. Experimental and theoretical stress-strain curves for unconfined steel-reinforced resin.

Table 2
Results for unconfined resin specimen.

Specimen	Young's Modulus* (GPa)	Strength (MPa)
U-R1	5.30	171.7
U-R2	6.15	168.9
U-R3	5.83	173.2
U-R4	5.45	168.7
U-R5	5.49	166.6
Mean	5.64	169.8
S.D.	0.34	2.62

* Determined in the range 20–60 MPa.

Table 3
Results for unconfined steel-reinforced specimen.

Specimen	Young's Modulus* (GPa)	Strength (MPa)
U-SR1	15.9	118
U-SR2	16.3	119.5
U-SR3	15.5	124.1
U-SR4	15.6	122.1
U-SR5	15.1	118.0
Mean	15.7	120.3
S.D.	0.41	2.72

* Determined in the range 40–80 MPa.

well as the predicted engineering stress-strain curves for the unconfined steel-reinforced resin specimen are illustrated through Fig. 9.

The density of each steel-reinforced specimen was determined, as well as the separate densities of the resin and shot. On average, it was found that $\rho_r = 1.86$ g/cm^3, $\rho_s = 7.49$ g/cm^3 and $V_f = 60\%$. The density and bulk density of the shot according to the supplier [31] is 7.4 g/cm^3 and 4.4 g/cm^3, respectively, leading to a volume fraction of 59.5%, which is consistent with the volume fraction obtained in the specimen.

3.2. Confined specimen

The engineering stress-strain curves for the confined resin and steel-reinforced resin specimen are illustrated through Figs. 10 and 11, respectively. The Young's Modulus of these specimen are summarized in Tables 4 and 5. Representative determination of Young's Moduli was done over an interval of 60 MPa (approximately one-third of the stress at the onset of non-linearity for confined resin specimen) for which the slope of the curve is largest, to avoid influence due to accuracy of recorded data. The non-linearity in the stress-strain diagram for the confined specimen is due to the yielding of the confining steel tube. Therefore the stress at the onset of non-linearity is a lower bound value.

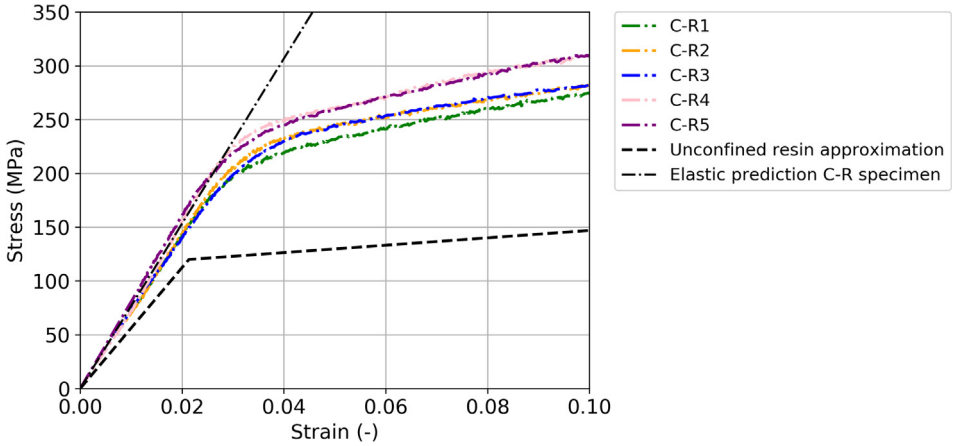

Fig. 10. Experimental stress-strain curves for confined resin, including prediction for Young's Modulus based on analytical model.

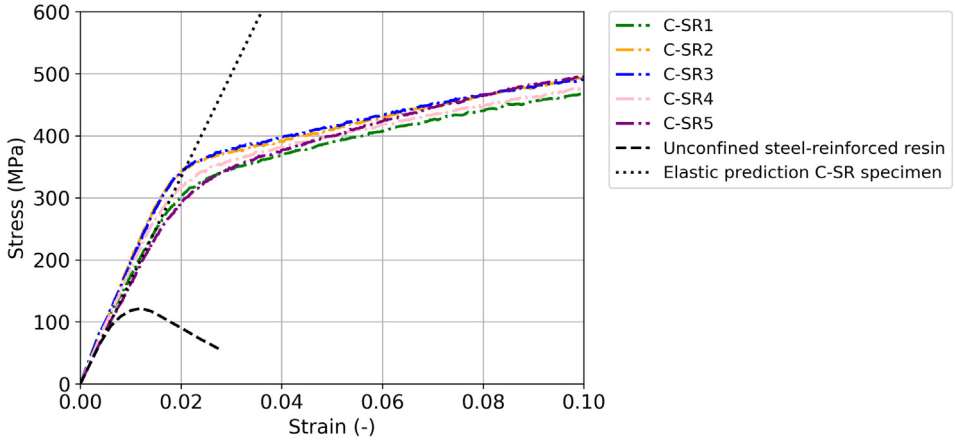

Fig. 11. Experimental stress-strain curves for confined steel-reinforced resin.

Table 4
Results for confined resin specimen.

Specimen	Young's Modulus* (GPa)
C-R1	7.2
C-R2	7.5
C-R3	6.6
C-R4	8.6
C-R5	7.9
Mean	7.6
S.D.	0.76

* Determined in the range 100–160 MPa.

Table 5
Results for confined steel-reinforced specimen.

Specimen	Young's Modulus* (GPa)
C-SR1	15.4
C-SR2	20.0
C-SR3	18.9
C-SR4	17.9
C-SR5	16.1
Mean	17.6
S.D.	1.9

* Determined in the range 150–210 MPa.

Fig. 12. Typical failure modes for resin (left) and steel-reinforced resin (right).

4. Discussion

4.1. Unconfined specimen

The Young's Modulus of the unconfined resin specimen shows little variation between different specimen (COV 6%). In addition, the stress at the onset of non-linearity and the maximum stress does not vary significantly either. The nominal strain at failure is in the range of 20%, indicating that the material is highly ductile. Prior to failure, longitudinal and diagonal cracks developed in the specimen. Final failure occurred through explosive spalling along these cracks, as illustrated through Fig. 12.

The unconfined steel-reinforced specimen show a significantly higher Young's Modulus (+178%) than the resin itself. The variation of the Young's Modulus for these specimen is in the same order of magnitude as the resin specimen (COV 3%). The ductility of the two-phase composite material is significantly decreased, with failure initiating through the formation of shear cracks at an average stress level of 120.3 MPa. The typical pattern of shear cracks is illustrated through Fig. 12.

The hybrid homogenization method developed to describe the behaviour of steel-reinforced resin overestimates the Young's Modulus by 5.7% as 16.6 GPa using the body-centred cubic unit cell. For the larger cell with a random sphere disposition, the average Young's Modulus for the steel-reinforced resin was determined as 16.7 GPa, with a coefficient of variation of 3% (originating from multiple subsamples within the larger cell). The average Young's Moduli based on two volumes of a (unit) cell chosen to evaluate the effect of sphere disposition do not vary significantly (difference < 1%). Therefore the assumption that a body-centred cubic packing of spheres is representative for the actual dispersion of spheres in a large volume of steel-reinforced resin is validated.

One of the reasons for the difference between actual and predicted Young's Modulus could be that the reinforcing spherical particles are not completely solid. According to SAE J827 [26], imperfections such as voids, shrinkage, cracks and deviations in particle shape are accepted to a certain extent. For example, no more than 10% of the particles may contain an internal hole that is larger than 10% of the cross-sectional particle area. Also, no more than 10% of the particles may contain an internal cavity as a result of shrinkage that is larger than 40% of the total area. The proposed hybrid homogenization model is adjusted such that the void/cavity in each particle can be included. Fig. 13 shows the Young's Modulus of the composite material as a function of the size of the relative area of the void/cavity within the particle, under the assumption that such defects always occur at the particle centre and have mechanical properties equal to that of the resin. From Fig. 13 it can be seen that such defects have the ability to decrease

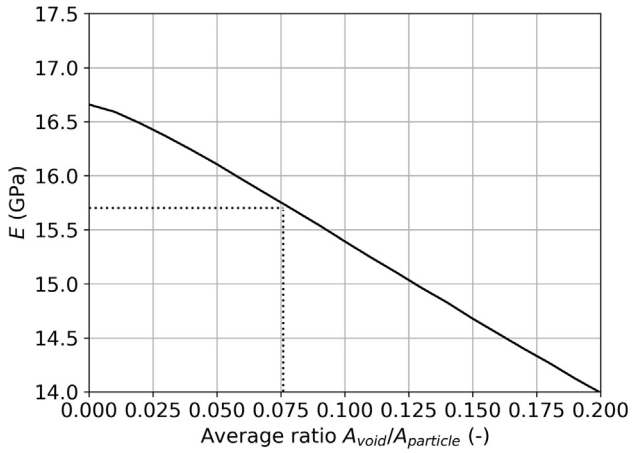

Fig. 13. Young's Modulus of steel-reinforced resin based on hybrid homogenization method as a function of the ratio of void area over total cross-sectional area. E_r = 5.64 GPa and V_f = 60%.

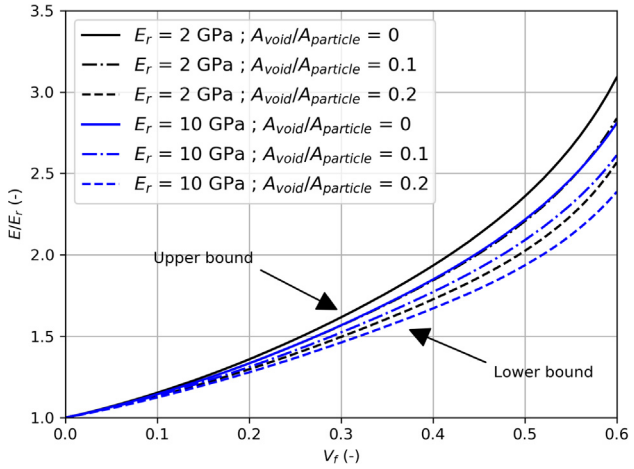

Fig. 14. Relative Young's Modulus of steel-reinforced resin as a function of void area ratio and Young's Modulus of resin.

mechanical properties to a level that was observed during the compression tests, i.e. with an average void with an area of approximately 7.5% of the cross-sectional particle area. This ratio of area corresponds to a void to particle volume ratio of (only) 2.1%.

The Young's Modulus of steel-reinforced resin as a function of the volume fraction is illustrated through Fig. 14, for resins with Young's Moduli of E_r = 2 GPa and E_r = 10 GPa and considering various ratios of the void area over total cross-sectional particle area. The chosen range of Young's Moduli is considered represent upper and lower bounds of Young's Moduli of (epoxy) resins. The relative increase in Young's Modulus due to the reinforcing particles does not vary significantly with Young's Modulus of the resin itself, nor with the ratio of void area over total cross-sectional particle area. From Fig. 14 it can be derived that, for steel-reinforced resin, the Young's Modulus is 240–310% of that of the conventional, unreinforced resin at a typical bulk volume fraction of 60%.

The descending branch of the stress-strain curve for the unconfined steel-reinforced specimen can be modelled using a phenomenological approach. The shear cracks indicate that the deformation of neighbouring elements is incompatible, e.g. due to the difference in lateral expansion. A simplified phenomenological damage model is derived that is based on each element individually. Given that the shear damage does not occur in resin alone, it logically follows that the damage model parameter D is

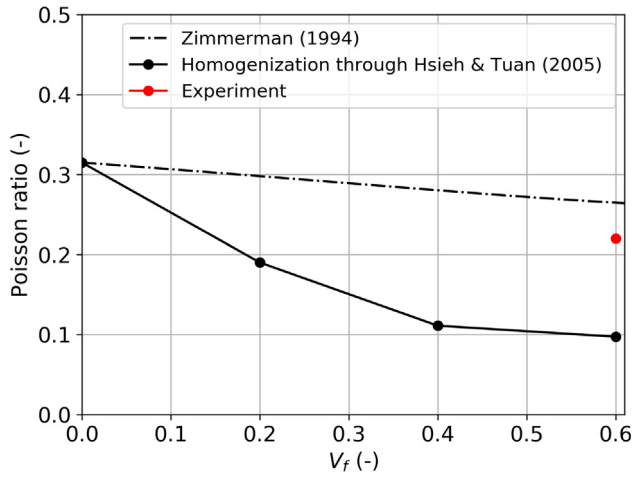

Fig. 15. Relationship between Poisson ratio and volume fraction of steel shot according to Zimmerman [29] and Hsieh & Tuan [30] for steel-reinforced resin. It is assumed that υ_s = 0.3 and υ_r = 0.315 (as determined experimentally).

a function of the strain of the resin and steel as expressed by Eq. (22) provided that $\varepsilon_s > 0$. The stress in a damaged element is assumed to decrease by a factor (1-D) to σ_D, see Eq. (23).

$$D = f(\varepsilon_r, \varepsilon_s) \tag{22}$$

$$\sigma_D = (1 - D) \cdot \sigma \tag{23}$$

The difference in strain between resin and steel is assumed to cause material damage if a certain threshold $\Delta\varepsilon_{thr}$, is exceeded, as expressed through Eq. (24). For simplification, it is assumed that the damage fully develops once the threshold is exceeded.

$$D(\varepsilon_r, \varepsilon_s) = \begin{cases} 1, & \text{if } |\varepsilon_r - \varepsilon_s| \geqslant |\varepsilon_{thr}| \text{ and } \varepsilon_s > 0 \\ 0, & \text{otherwise} \end{cases} \tag{24}$$

The constant $\Delta\varepsilon_{thr}$ is determined through fitting as $\Delta\varepsilon_{thr}$ = 0.07. The predicted stress-strain curve of the composite material including damaged material behaviour is illustrated through Fig. 9. Although the proposed damage model may not be fully physically explainable, it indicates that the damage is dependent on the strain difference. Since in the actual application this damage phenomenon is not observed due to strong confinement conditions, the damage model is not extensively expanded.

The experimentally established Poisson ratio of 0.22 for steel-reinforced resin could not be replicated analytically, neither by the model of Zimmerman [29] (υ = 0.265 see Fig. 15), nor through the model of Hsieh & Tuan [30] (υ = 0.097, see Fig. 15) that was implemented in the hybrid homogenization method. Deviation between predictions and experimental value is not surprising, given the wide bounds that exist in literature for the Poisson ratio of two-phase composites and that determination of the Poisson ratio of two-phase composite materials is an often-neglected issue [30]. As a safe approximation, a Poisson ratio of 0 may be adopted in combination with a Young's Modulus based on unconfined (conservative approximation) or confined (realistic approximation) test results

5. Confined specimen

The confined resin specimen showed an increase in (apparent) Young's Modulus of 35% that matched well with the prediction based on the analytical model (+36%), as illustrated through Fig. 6. The same goes for the increase in apparent Young's Modulus of +12% for confined steel-reinforced resin specimen compared to a

prediction of a 10.3% increase. The coefficient of variation for the confined specimen is approximately 10%, and is larger than that of the unconfined specimen (3–6%). A possible explanation for this increase is that the coefficient of variation is influenced by the uncertainties that exist within the confining cylinder, i.e. its thickness and Young's Modulus.

Due to the confinement, the specimen could withstand significantly higher stresses and strains than specimen in unconfined condition. The non-linear branch of the stress-strain curve is due to yielding of the confining cylinder: this leads to the situation where the resin is no longer restrained to lateral deformation. The complex behaviour in this phase (yielding of cylinder, and consequently reduction of confinement) makes it difficult to distinguish between the different phenomena (yielding of cylinder and non-linear behaviour of specimen). Therefore, it is recommended to repeat the series of confined tests using thicker and stronger steel cylinders, in order to capture the true non-linear specimen behaviour. It is the specimen behaviour that will govern the behaviour in real applications, since generally the (steel-reinforced) resin is in a bolt hole which has a relatively large edge and pitch distances and thus yielding of the confining element is not relevant.

6. Conclusion

The main outcomes of the discussion above are as follows:

- The stress-strain relationship of steel-reinforced resin could be predicted well using the derived hybrid homogenization model. The mean difference between experimental and theoretical Young's Modulus is less than 6%.
- The gravitation principle of Gravitational Sphere Packing Method was combined with 3D simulation software, to generate random sphere distributions. This combined method does not require user-defined algorithms to deal with contact interactions and is therefore straightforward to implement.
- Using random sphere dispositions generated through the method outlined above, it was proven that the Young's Modulus of steel-reinforced resins with randomly distributed, equally sized spheres can be accurately predicted (difference < 1%) using a sphere disposition based on a body-centred cubic packing.
- The Young's Modulus of steel-reinforced resin is approximately 140–210% higher than that of non-reinforced resin for a typical bulk volume fraction (60%) of reinforcing steel spheres.
- The positive effects of confinement on the mechanical properties (increase in stiffness and strength) increase rapidly with increasing Poisson ratio. The boundary conditions (diameter, thickness, Young's Modulus of the confining cylinder) have a less pronounced effect for decreasing Young's Moduli of the confined material.
- The Poisson ratio of steel-reinforced resin could not be determined with sufficient accuracy using two existing analytical models – more in-depth research is required to make an accurate prediction of the Poisson ratio of steel-reinforced resins.

Further research

Present model could further be extended, e.g. by including a (pressure-dependent) yield criterion to obtain a non-linear prediction for the confined specimen or by including the creep deformation of the resin to capture the effective mechanical properties on the long term.

Conflict of interest

The authors declared that there is no conflict of interest.

Acknowledgement

This research was carried out under project number T16045 in the framework of the Partnership Program of the Materials Innovation Institute M2i (www.m2i.nl) and the Technology Foundation TTW (www.stw.nl), which is part of the Netherlands Organization for Scientific Research (www.nwo.nl).

References

[1] J. de Oliveira Correia, B. Pedrosa, P. Raposo, A. De Jesus, H. dos Santos Gervasio, G. Lesiuk, L. da Silva, Fatigue strength evaluation of resin-injected bolted connections using statistical analysis, Engineering 3 (6) (2017) 795–805.
[2] NEN, EN1993-1-8 – Eurocode 3: Design of Steel Structures – Part 1-8: Design of Joints, Delft: NEN, 2005.
[3] M.P. Nijgh, M. von Arnim, M. Pavlovic, M. Veljkovic, Preliminary assessment of a composite flooring system for reuse, in: 8th International Conference on Composite Construction in Steel and Concrete, Jackson, WY, 2017.
[4] A. Koper, Assessment of Epoxy Resins for Injected Bolted Shear Connections, Delft University of Technology, Delft, 2017.
[5] F. Wedekamper, Avaliação de resinas epóxi para aplicação em end fittings de dutos flexíveis, Universidade Federal do Rio Grande do Sul, Rio Grande, 2017.
[6] M.P. Nijgh, New Materials for Injected Bolted Connections – A Feasibility Study for Demountable Connections, Delft University of Technology, Delft, 2017.
[7] W. Voigt, Ueber die Beziehung zwischen den beiden Elasticitätsconstanten isotroper Körper, Ann. Phys. 274 (1889) 573–587.
[8] A. Reuss, Berechnung der Fließgrenze von Mischkristallen auf Grund der Plastizitätsbedingung für Einkristalle, Zeitschrift für Angewandte Mathematik und Mechanik 9 (1929) 49–59.
[9] G. Dvorak, Y. Behei-El-Din, Plasticity analysis of fibrous composites, J. Appl. Mech. 49 (2) (1982) 327–335.
[10] Z. Hashin, On elastic behaviour of fibre reinforced materials of arbitrary transverse phase geometry, J. Mech. Phys. Solids 13 (3) (1965) 119–134.
[11] Z. Hashin, The elsatic moduli of heterogeneous materials, J. Appl. Mech. 29 (1) (1962) 143–150.
[12] Z. Hashin, S. Shtrikman, A variational approach to the theory of the elastic behaviour of multiphase materials, J. Mech. Phys. Solids 11 (2) (1963) 127–140.
[13] Z. Hashin, S. Shtrikman, Note on a variational approach to the theory of composite elastic materials, J. Franklin Inst. 271 (4) (1961) 336–341.
[14] R. Hill, A self-consistent mechanics of composite materials, J. Mech. Phys. Solids 13 (4) (1965) 213–222.
[15] J. Eshelby, The determination of the elastic field of an ellipsoidal inclusion, and related problems, Proc. R. Soc. Lond. A241 (1226) (1957) 376–396.
[16] T. Mori, K. Tanaka, Average stress in matrix and average elastic energy of materials with misfitting inclusions, Acta Metall. 21 (5) (1973) 571–574.
[17] Y. Benveniste, A new approach to the application of Mori-Tanaka's theory in composite materials, Mech. Mater. 6 (2) (1987) 147–157.
[18] J. Fish, Practical Multiscaling, John Wiley & Sons, 2013.
[19] H. Xin, S. Sun, J. Fish, A surrogate modeling approach for additive-manufactured materials, Int. J. Multiscale Comput. Eng. 15 (6) (2017) 525–543.
[20] H. Xin, Y. Liu, A.S. Mosallam, J. He, A. Du, Evaluation on material behaviors of pultruded glass fiber reinforced polymer (GFRP) laminates, Comp. Struct. 182 (2017) 283–300.
[21] H. Xin, W. Sun, J. Fish, Discrete element simulations of powder-bed sintering-based additive manufacturing, Int. J. Mech. Sci. (2017).
[22] Y. Shi, Y. Zhang, Simulation of random packing of spherical particles with different size distributions, Appl. Phys. A 92 (2008) 621–625.
[23] H. Kitti, M. Bernacki, Optimized Dropping and Rolling (ODR) method for packing of poly-disperse spheres, Appl. Math. Model. 37 (2013) 5715–5722.
[24] M. Roozbahani, B. Huat, A. Asadi, Effect of rectangular container's sides on porosity for equal-sized sphere packing, Powder Technol. 224 (2012) 46–50.
[25] Blender Foundation, Blender 3D Computer Graphics Software (v. 2.79b), Amsterdam, 2018.
[26] SAE International, J827: High-Carbon Cast-Steel Shot, SAE International, 2013.
[27] SAE International, J444: Cast Shot and Grit Size Specifications for Peening and Cleaning, SAE International, 2012.
[28] J. Williams, C. Gamonpillas, Using the simple compression test to determine Young's modulus, Poisson's ratio and the Coulomb friction coefficient, Int. J. Solids Struct. 45 (16) (2008) 4448–4459.
[29] R. Zimmerman, Behaviour of the poisson ratio of a two-phase composite material in the high-concentration limit, Appl. Mech. Rev. 47 (1) (1994) S38–S44.
[30] C. Hsieh, W. Tuan, Poisson's ratio of two-phase composites, Mater. Sci. Eng. A 396 (1–2) (2005) 202–205.
[31] Airblast Abrasives, High Carbon Steel Shot & Grit, May 2016. [Online]. Available: https://www.airblast.com/media/org/7a0d659705c5f406783680e38fafd070.pdf. (Accessed 28 March 2018).